ACS Synthetic Biology

pubs.acs.org/synthbio Research Article

Cell-Free Synthesis Goes Electric: Dual Optical and Electronic Biosensor via Direct Channel Integration into a Supported Membrane Electrode

Zachary A. Manzer,[‖] Surajit Ghosh,[‖] Arpita Roy, Miranda L. Jacobs, Juliana Carten, Neha P. Kamat, and Susan Daniel*

Cite This: *ACS Synth. Biol.* 2023, 12, 502−510 Read Online

ACCESS | Metrics & More | Article Recommendations | Supporting Information

ABSTRACT: Assembling transmembrane proteins on organic electronic materials is one promising approach to couple biological functions to electrical readouts. A biosensing device produced in such a way would enable both the monitoring and regulation of physiological processes and the development of new analytical tools to identify drug targets and new protein functionalities. While transmembrane proteins can be interfaced with bioelectronics through supported lipid bilayers (SLBs), incorporating functional and oriented transmembrane proteins into these structures remains challenging. Here, we demonstrate that cell-free expression systems allow for the one-step integration of an ion channel into SLBs assembled on an organic conducting polymer, poly(3,4-ethylenedioxythiophene) polystyrenesulfonate (PEDOT:PSS). Using the large conductance mechanosensitive channel (MscL) as a model ion channel, we demonstrate that MscL adopts the correct orientation, remains mobile in the SLB, and is active on the polyelectrolyte surface using optical and electrical readouts. This work serves as an important illustration of a rapidly assembled bioelectronic platform with a diverse array of downstream applications, including electrochemical sensing, physiological regulation, and screening of transmembrane protein modulators.

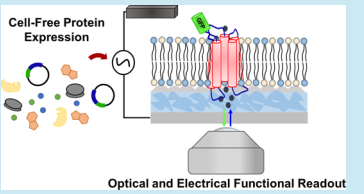

KEYWORDS: *cell-free protein synthesis, membrane protein, bioelectronic, supported lipid bilayer, dual-readout*

INTRODUCTION

Membrane proteins are important regulators of cellular homeostasis, mediating the transport of information and materials across cellular membranes. The ability to recapitulate these electrochemical functions achieved by biology on material devices opens the door to a variety of technological applications, from implantable devices to wearable sensors to platforms for drug screening.[1−3] To harness specific membrane functions, biological membrane components need to be interfaced with abiotic materials in a manner that maintains their native behavior.

Conjugated polymers, such as poly(3,4-ethylenedioxythiophene) polystyrenesulfonate (PEDOT:PSS), have emerged as a standard bioelectronic interface material due to their biocompatibility, optical transparency, and ease of use.[4] Several biological molecules, including peptides, polysaccharides, and even living cells have been conjugated to these material surfaces in order to bridge biological sensing functions to electronic readouts.[2,5,6] However, transmembrane proteins (TMPs) are one class of biomolecules that have historically been the most challenging to interface with bioelectronic platforms. Maintaining the structural and functional properties of TMPs requires a specific environment, namely, a lipid bilayer, that allows the proteins to adopt their proper structure and diffuse within the membrane to interact with other proteins and lipids. It has been a challenge in the field to recreate the appropriate membrane environment on electronic interfaces that preserve TMP activity.

Supported lipid bilayers (SLB) assembled on the surface of conducting polymers provide a unique solution to couple TMP activity with electronic interfaces.[7] SLBs are planar, supported membranes that are compatible with various surface analytical techniques.[8−11] Importantly, SLBs can be used to coat electrodes with a lipid membrane to translate biological activity into electrical readouts.[10,12−15] While the direct deposition of cell membranes on PEDOT surfaces has provided a promising strategy to interface lipid bilayers and TMPs onto electronically active materials,[10,16] biological membranes are highly complex, which can confound measurement signals. Additionally, these methods can have a lengthy development timeline, are often costly, and require specialized equipment and reagents. Hence, developing methods to rapidly and efficiently integrate TMPs into SLBs on electrically responsive devices with defined components is of importance

Received: October 8, 2022
Published: January 18, 2023

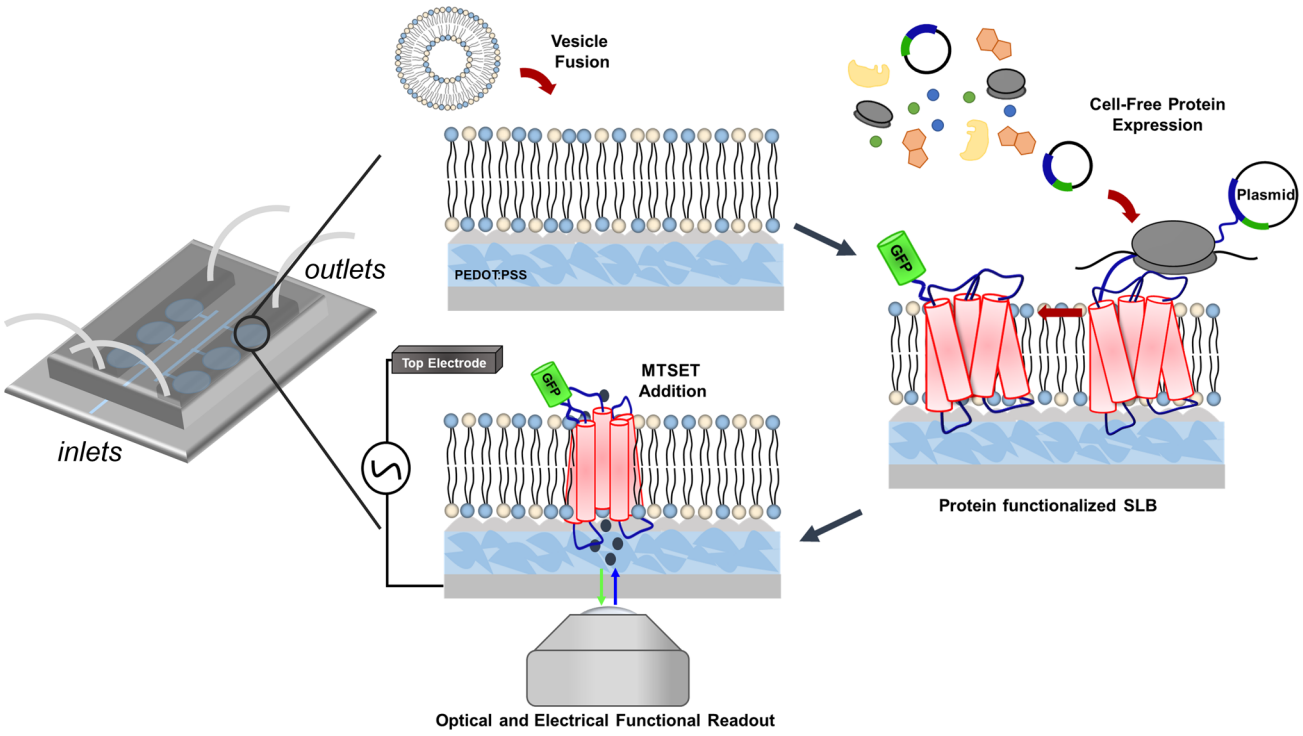

Figure 1. Schematic representation of the cell-free bioelectronic sensor. The modular nature of cell-free protein synthesis enables electrodes to be created in an array and integrated with microfluidics. The sensing environment is created after supported lipid bilayer (SLB) formation from the fusion of synthetic liposomes to the surface and then in a single step co-translational insertion of protein directly into a preformed SLB on a bioelectronic platform. The SLB provides a biomimetic interface to retain protein activity, while the conductive, transparent polymer support (PEDOT:PSS) allows both optical and electrical measurements to be conducted. The final configuration allows an electrical circuit to be established wherein changes in protein activity can be measured using electrochemical impedance spectroscopy. Note that the protein and supported membrane are not drawn to scale.

to the field and will ultimately enable more complex and precise biosensing platforms to be developed.

An emerging route to rapidly assemble TMPs into an SLB is co-translational integration, in which TMPs are synthesized directly into a lipid membrane.[17] By supplementing these cell-free protein synthesis (CFPS) reactions with synthetic membranes, like nanodiscs and liposomes, the traditional challenges in TMP expression are circumvented. These include both the long and laborious method for TMP synthesis and purification, as well as the need to disrupt native folding through detergent extraction. The modular nature of CFPS allows the protein synthesis and the reaction environment to be engineered to create novel synthetic biology tools.[17] Even further, this enables the synthesis of difficult-to-express proteins, including those that are cytotoxic. This approach has been successfully used to generate membrane-spanning TMPs for both basic structural measurements[18] and biosensing in 2D-supported membranes.[19] Unlike more common methods that use detergent-mediated reconstitution of purified proteins, CFPS retains the native cellular machinery and allows for the direct insertion of proteins into a bilayer as they are produced. This approach minimizes both the number of steps required to assemble the TMP-integrated bilayer as well as the use of detergents, which can change membrane properties and correspondingly affect TMP function. Furthermore, the use of CFPS can enable the oriented integration of TMPs into SLBs compared to reconstitution methods. TMPs typically must thread through the membrane multiple times and therefore need to be oriented correctly. Recreating the proper orientation of a given TMP within the membrane is important, as this can impact the protein's interactions with the underlying electronic materials, mobility within the bilayer, and function (e.g. the directional transport of ions or signal transduction).

Recently, we used CFPS to demonstrate the synthesis of the large conductance mechanosensitive channel (MscL) into a fluid hybrid-supported lipid bilayer (HSLB) containing phospholipids and diblock copolymers.[20] MscL is a well-characterized bacterial pore-forming membrane protein, composed of five subunits, that senses and dissipates physical stresses in cell membranes.[21] We reported the expression, proper folding and orientation, and mobility of this ion channel by monitoring a fluorescent reporter (GFP) covalently linked to this membrane protein. The readouts for these attributes were straightforward to assess using fluorescence microscopy as the HSLBs were formed on transparent glass supports. However, glass supports are electrically insulating and thus preclude measuring ion flux across the SLB, and we could not measure ion channel activity directly in this system. To solve this problem, we used cell-free integration of the same ion channel (MscL) into an SLB on a conducting polymer film and then optically and electrically recorded small molecule transport mediated by this channel.

We report here the cell-free co-translational synthesis of an ion channel, MscL, into a supported lipid bilayer on a conducting polymer film. Specifically, we used a PEDOT:PSS film on ITO electrodes and measured ion flux across the supported membrane through the embedded ion channels (Figure 1). In addition to the conducting polymer enabling electrical readouts, PEDPT:PSS is transparent, making this

https://doi.org/10.1021/acssynbio.2c00531
ACS Synth. Biol. 2023, 12, 502−510

electrical device compatible with optical measurements using fluorescence microscopy, making this a dual modality sensor. Another attractive feature of the conducting polymer is that it acts as a hydrated hydrogel cushion that enables TMP mobility throughout the supported lipid bilayer—a necessary feature for some TMP functions. Following device fabrication, we co-translationally integrated MscL proteins into the SLB and measured their transport properties using fluorescence microscopy and electrochemical impedance spectroscopy (EIS). We used two different versions of MscL to detect a differential response to exposure of 2-(trimethylammonium)-ethyl methanethiosulfonate, bromide (MTSET). The wild type (WT-MscL) is not responsive to MTSET, while a cysteine modification enables the channel to open (G22C-MscL). This illustrates the ability to directly read out the activity of individual membrane proteins and discriminate them based on a differential electrical response. Integrating functional TMPs with a multimodal bioelectronic membrane platform is an important advancement in biosensor capabilities as we move closer to the goal of creating high-throughput designer biosensors with broad applications across medical, manufacturing, pharmaceutical, and research sectors.

EXPERIMENTAL SECTION

Materials. 1-Palmitoyl-2-oleoyl-glycero-3-phosphocholine (16:0−18:1 PC, POPC) and 1-palmitoyl-2-oleoyl-*sn*-glycero-3-phospho-(1′-rac-glycerol) (sodium salt) (POPG) were obtained from Avanti Polar Lipids (Alabaster, AL, USA). Texas Red 1,2-dihexadecanoyl-*sn*-glycero-3-phosphoethanolamine, triethylammonium salt (TR-DHPE), 2-(trimethylammonium)ethyl methanethiosulfonate, bromide (MTSET), and octadecyl rhodamine 123 (R18) were obtained from Thermo Fisher Scientific. All of these chemicals were used without further purification. PEDOT:PSS (Clevios PH 1000) was obtained from Heraeus Clevios GmbH. 4-Dodecylbenzenesulfonic acid (DBSA), (3-glycidyloxypropyl) trimethoxysilane (GOPS), ethylene glycol (EG), polyallylamine hydrochloride (PAH), poly-L-lysine (PLL), and phosphate-buffered saline (PBS) were purchased from Sigma-Aldrich (St. Louis, MO, USA). Patterned ITO electrodes on glass substrates were purchased from Xin Yan Technology Limited (China).

Plasmid Information. Plasmids used here have been described previously.[20,22] pET19b-EcMscL and pET19b-EcMscL-G22C were used for cell-free synthesis into supported bilayers coating ITO-PEDOT:PSS sensors. MscL is natively a mechanosensitive channel, but the G22C mutation allows for specific chemical channel activation via the addition of MTSET, which reacts with the cysteine mutation.[23] For fluorescence tracking, we used pET19b-EcMscL-mEGFP which is C-terminally tagged by the monomeric enhanced green fluorescent protein (mEGFP). A Tobacco Etch Virus (TEV) protease cleavage site is located between MscL and GFP for post-synthesis GFP removal. All plasmids contain the T7 promoter to enable robust cell-free gene expression.

Small Unilamellar Liposome Preparation. Small unilamellar liposomes of POPC and POPG (1:1 mol %) were prepared using thin-film hydration and extrusion methods. The required amounts of POPC and POPG dissolved in $CHCl_3$ were mixed in glass vials to achieve the desired mole percentage. $CHCl_3$ was evaporated using a stream of nitrogen gas to form a thin phospholipid film, and the glass vial was kept in a vacuum for a minimum of 4 h to remove trace amounts of $CHCl_3$, if present. Eventually, the lipid films were rehydrated with 300 mOsm PBS to a concentration of 2 mg/mL, vortexed to resuspend the phospholipids completely, and extruded 10 times through a 50 nm Nucleopore polycarbonate membrane using an Avanti Extruder (Avanti Polar Lipids, Birmingham, AL).

Characterization of Phospholipid Liposomes. The average hydrodynamic size and zeta potential of phospholipid liposomes in 300 mOsm PBS were monitored on a Zetasizer Nano-ZS instrument (Malvern Instruments) with a 4 mW He−Ne laser (λ = 632 nm) and backscattered detector angle 173°. Liposomes were approximately 75 ± 5 nm in diameter with a zeta potential of −30 ± 3 mV in 300 mOsm PBS (Figure S1, Supporting Information).

Preparation of PEDOT:PSS Suspension. Ninety-five percent v/v Clevios PH 1000 (Heraeus), 5% v/v ethylene glycol, 1% v/v (3-glycidyloxypropyl)trimethyoxysilane, and 0.002% v/v 4-dodecylbenzenesulfonic acid (DBSA) were mixed together in a glass vial. The mixture was then placed in a bath sonicator (ultrasonic cleaner, VWR) for ∼0.5 h. Prior to use, the solution mixture passed through a 0.45 μm syringe filter (Thomas Scientific).

Glass/PEDOT:PSS Slide/ITO Electrode Preparation. A microscope cover glass (25 mm × 25 mm; No. 1.5; VWR) was cleaned using a 70% sulfuric acid (H_2SO_4) and 30% hydrogen peroxide (H_2O_2) solution mixture for 10 m and then washed with deionized water (18.2 MΩ cm) for 0.5 h. After that, the glass slides were kept in deionized water and just prior to use, and these slides were dried with a stream of nitrogen gas and used immediately to assemble supported lipid bilayers.

To prepare PEDOT:PSS films, washed glass slides or patterned ITO electrodes were briefly rinsed with deionized water and dried with a stream of nitrogen gas before being plasma-cleaned at 29.6 W and 700 micrometer pressure for 2 min (Harrick Plasma, Ithaca, NY). The plasma-cleaned glass slides were then coated with the PEDOT:PSS suspension at 2500 rpm for 30 s using a spin-coater (Apogee Spin coater, Cost Effective Equipment). The PEDOT:PSS-coated slides were baked at 140° for 1 h and then immersed in DI water for ∼4 h. Finally, before use, these slides were dried with a stream of nitrogen gas and treated with oxygen plasma at 29.6 W and 700 micrometer pressure for 2 min.

Supported Lipid Bilayer Formation. Cleaned glass/PEDOT:PSS coated slides/electrodes were used as a solid surface for SLB formation. First, PDMS (polydimethylsiloxane, 10:1 elastomer: cross-linker mixture of Sylgard 184) wells (with average area of ∼1 cm^2) were attached to a glass/PEDOT:PSS slide. PEDOT:PSS is negatively charged, so it requires a thin coating of either PAH or PLL, positively charged polyelectrolytes, to promote the rupture POPC-POPG liposomes on this surface. To prepare the PAH-coated glass slide or ITO device, first, 80−100 μL of PAH solution (concentration 1−2 mg/mL) in 0.5 M NaCl solution was added to the well and incubated for 15−20 min. The unabsorbed PAH was washed with DI water and then with PBS buffer. Poly-L-lysine (PLL) was used directly from the manufacturer without modification in place of PAH for protein imaging. This substitution was made to reduce background noise in single particle tracking. Eighty microliters of liposome solution at ∼0.5 mg/mL concentration was then added into the well and incubated for 15−20 min for the absorption and subsequent rupture of liposomes to form contiguous SLBs.

https://doi.org/10.1021/acssynbio.2c00531
ACS Synth. Biol. 2023, 12, 502−510

Finally, the well was rinsed with PBS to remove excess unruptured liposomes.

Fluorescence Recovery after Photobleaching Measurements. The formation of a fluid supported lipid bilayer on the surface was monitored by fluorescence recovery after photobleaching (FRAP) of a fluorescently labeled phospholipid, TR-DHPE (~1.0 mol %). TR-DHPE was added into a mixture of POPC-POPG lipids before resuspension into PBS to provide labeled liposomes for FRAP analysis. The FRAP instrument consisted of an inverted Zeiss Axio Observer Z1 microscope containing an α Plan-Apochromat 20× objective and a 150 mW 561 nm optically pumped semiconductor laser (Coherent, Inc). The laser bleached a ~20 μm diameter spot, and then the recovery of the bleached spot's intensity was recorded over time. After background subtraction and normalization for photobleaching effects, fluorescence intensity recovery data was fit to the 2D diffusion equation following the method of Soumpasis et al.[24] The following equation was used to calculate the diffusion coefficient (D).

$$D = \frac{w^2}{t_{1/2}} \tag{1}$$

where w denotes radius of the photobleached spot and $t_{1/2}$ represents the time required to achieve half of the maximum recovery intensity.

Cell-Free Protein Synthesis. CFPS was performed using a PURExpress In Vitro Protein Synthesis kit (E6800) from New England Biolabs, Inc. (Ipswich, MA). We followed the manufacturer's protocol for protein expression using 200 ng of plasmid per 30 μL of reaction volume; however, we augmented the system by conducting the reaction in the presence of SLBs. We used 0.5 mg/mL liposomes in PBS for SLB fabrication on PAH-coated glass/PEDOT:PSS. After formation of the SLBs, wells were rinsed with PBS and then autoclaved DI water to remove the unruptured liposomes and salts. The CFPS reaction was then added to the surface of the SLB and incubated at 37 °C for 30−40 min; afterward, the SLBs were rinsed with PBS to stop the reaction.

Cleavage Assay for Protein Orientation. The orientation of MscL-GFP in the SLBs was determined using a TEV protease (New England Biolabs, Inc.) assay according to the manufacturer's protocols (1:10 dilution of TEV protease and incubation at 30 °C for 1 h) to cleave the GFP molecules from MscL after insertion into the SLBs.[20] We used total internal reflection fluorescence (TIRF) microscopy to quantify fluorescent GFP particles before and after TEV protease treatment. Samples were incubated with TEV protease overnight in the dark at 4 °C to prevent photobleaching of GFP molecules, and cleaved GFP molecules were rinsed away with PBS before imaging. We used ImageJ (NIH) to count the fluorescent punctate particles.[25] To provide better visual clarity of punctate spots, the contrast was modified slightly in the presented images but the images were left unmodified for all analyses.

Mobility Characterization of Individual Membrane Proteins. The mobility of MscL-GFP molecules in SLBs were determined using TIRF microscopy on an inverted Zeiss Axio Observer Z1 microscope with an α Plan-Apochromat 100× objective. A 561 nm solid-state laser was utilized to excite GFP molecules for tracking. A Laser TIRF 3 slider (Carl Zeiss, Inc.) was used to control the incident angle to create an evanescent wave of ~100 nm. A Semrock LF488-B-ZHE filter cube was used to filter excitation light that was then sent to the electron-multiplying CCD camera (ImageEM C9100−13, Hamamatsu). All images were analyzed using ImageJ (NIH) and Matlab (Mathworks).

EIS Measurements. Impedance spectra were recorded using a Potentiostat (Autolab PGSTAT128N) equipped with a frequency response analysis module. A commercially available Ag/AgCl electrode and a platinum mesh were used as reference and counter electrodes, respectively. PEDOT:PSS-coated ITO electrodes were used as working electrodes, with average areas of ~0.5 cm^2. MTSET was added to the samples at a final concentration of 10 μM for roughly 15 min before rinsing with PBS. EIS was monitored within the 100,000 to 0.1 Hz frequency range with an applied AC voltage of 0.01 V and a DC voltage of 0 mV versus OCP (open circuit potential). The measured impedance spectra were fit to a model using the Metrohm Autolab NOVA 2 software. Specifically, the model consists of a resistor and capacitor for the electrolyte and PEDOT:PSS-coated electrode, respectively, and a resistor and capacitor in parallel for the SLB.[26] This model was chosen based on inherent properties of the SLB, as has been discussed previously.[27]

RESULTS AND DISCUSSION

A Cationic Surface Coating Enables Assembly of Fluid SLBs on PEDOT:PSS Surfaces. To maximize the sensitivity of our transmembrane ion channel biosensing platform, we first needed to successfully form SLBs on an electrode surface of low impedance. PEDOT:PSS is a biocompatible conducting polymer that, when coated on electrode surfaces, has been shown to drastically reduce their impedance.[28,29] However, the surface charge of PEDOT:PSS is negative at neutral pH, which poses a challenge for the adsorption, rupture, and self-assembly of SLBs made with anionic lipids. Negatively charged lipids, such as POPG, are commonly found in bacterial membranes where many ion channels like MscL typically reside. To make the surface more amenable to negatively charged liposome rupture and the self-assembly of SLBs, we deposited a broadly used, nanometer-scale cationic polyelectrolyte layer on the surface prior to liposome addition.[30−34] These coatings do provide an additional electrical resistance, but this effect is minimal compared to the addition of the SLB and protein activity.

We confirmed the formation and fluidity of POPC−POPG bilayers on polyallylamine hydrochloride (PAH)-coated glass or PEDOT:PSS surfaces using fluorescence recovery after photobleaching (FRAP). FRAP experiments were conducted with a POPC-POPG bilayer containing 1 mol % of the fluorescently labeled phospholipid TR-DHPE. We carried out these FRAP experiments using several comparative surfaces. First, we demonstrated that without the cationic electrolyte coating on either glass or PEDOT:PSS, these anionic liposomes are not able to rupture and self-assemble into a SLB, as evidenced from the lack of fluorescence recovery after photobleaching (Figure S2A,B). However, on PAH-coated glass, we observed POPC−POPG liposome rupture and fluorescence recovery after photobleaching (Figure S2C). We obtained a diffusion coefficient of TR-DHPE as ~0.60 ± 0.10 μm^2/s with a mobile fraction of 0.99 ± 0.02 (Figure S3). Finally, for PAH-coated PEDOT:PSS surfaces, we also observed liposome rupture and fluorescence recovery. Figure S2D−F shows the FRAP images, the intensity data, and the fits of these data to the 2D diffusion model. From this fit, we

https://doi.org/10.1021/acssynbio.2c00531
ACS Synth. Biol. 2023, 12, 502−510

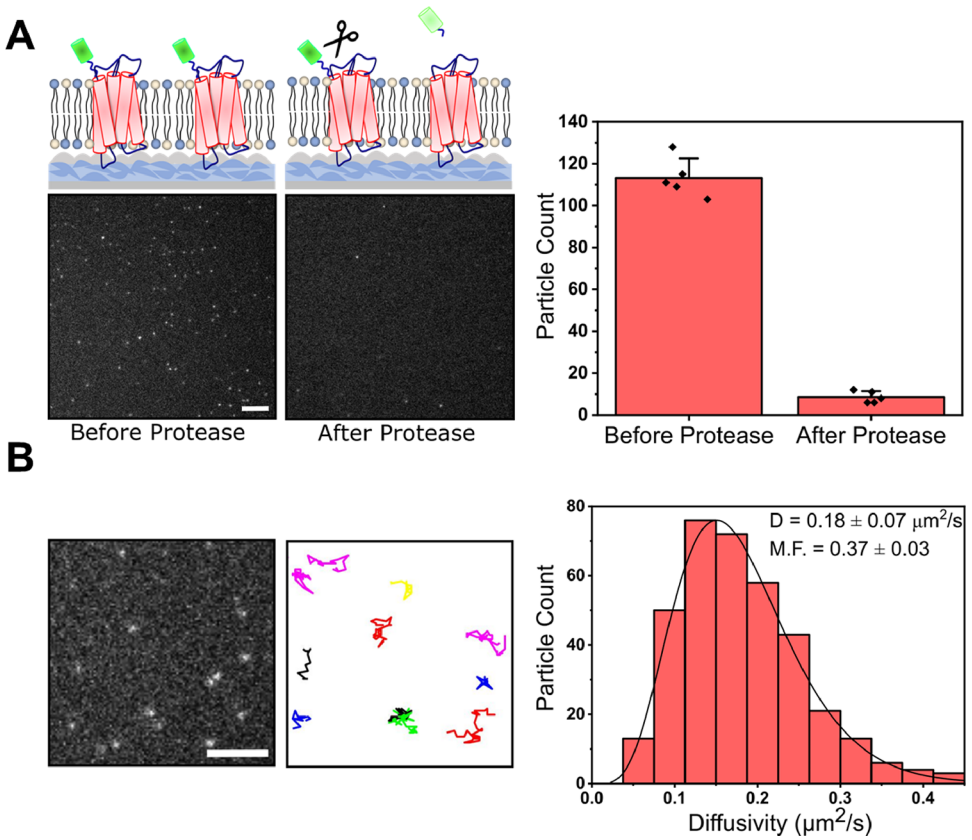

Figure 2. The nascent MscL-GFP proteins incorporated into SLBs using cell free protein synthesis are uniformly oriented and mobile. (A) Fluorescence microscopy images of an SLB containing MscL-GFP before and after TEV protease treatment. Individual white spots represent detected GFP fluorescence (scale bar is 10 μm). Treatment with TEV protease results in the nearly complete loss of GFP fluorescence from the SLB. Total protein counts were quantified before and after protease treatment (error bars represent standard error of the mean, n = 5). (B) Representative image of a SLB used to trace the trajectory of mobile MscL-GFP particles (scale bar is 5 μm). Mean square displacement measurements were made using the first three time points and fit to a Gaussian distribution to find the overall diffusivity and mobile fraction of MscL-GFP.

calculate the diffusion coefficient of TR-DHPE in a POPC-POPG bilayer as ~0.56 ± 0.09 μm^2/s with a mobile fraction of 0.94 ± 0.02. The fluorescence recovery in both cases confirms that the liposomes adsorbed to the cationic surfaces and ruptured to form a contiguous SLB at least over the length scale of the bleach spot. Additionally, similar diffusion coefficients between the PAH-coated glass and PAH-coated PEDOT:PSS indicate that the PEDOT:PSS polymer does not affect the diffusion coefficient or mobile fraction of lipid molecules in the SLB supported by it. A set of data from three experiments for each surface is provided in Figure S4 of the Supporting Information.

Cell-Free Expression of MscL Results in Oriented, Diffusive Proteins in SLBs Supported on PEDOT:PSS Surfaces. After verifying the formation of mobile SLBs on PEDOT:PSS surfaces, we investigated the cell-free synthesis approach to integrate ion channels into these SLBs. We measured two figures of merit for proteins: orientation and mobility. Both factors confirm the state of the synthesized protein as well as the presence of a mobile SLB. Protein orientation is an important indicator of function as it can influence the direction of ion transport in certain protein channels. Here, we used the mechanosensitive channel of large conductance (MscL) and cell-free methods to co-translationally insert MscL into a phospholipid bilayer containing anionic and zwitterionic phospholipids on PEDOT:PSS-coated ITO electrodes. Once the devices were formed and MscL's orientation and mobility in the bilayer were confirmed, we electrically assessed its ion flux activity.

To first characterize both protein synthesis and orientation, we used a fluorescence-based assay. We used a poly-(L)-lysine (PLL) coating on the glass surfaces as we observed high background fluorescence from the PAH coating on PEDOT:PSS. We synthesized MscL with a C-terminal GFP tag containing a TEV cleavage sequence between MscL and GFP (MscL-GFP). This construct design achieved two goals: first, we can readily observe protein synthesis by the emergence of fluorescence as the synthesis reaction proceeds via the GFP folding reporter. Second, we can assess orientation of the synthesized proteins by cleaving GFP after synthesis and monitoring the subsequent loss in fluorescence. To assist in quantification, we carried out the CFPS reaction over the pre-formed SLB until we could identify single fluorescent particles and then stopped the reaction by rinsing the surface with PBS buffer and removing the reactants and plasmids from the bulk phase. Individual fluorescent spots corresponding to MscL-GFP are shown in a representative image (Figure 2A), indicating successful expression and, most likely, folding of the channel.[20,35,36]

After confirming that the CFPS system had generated MscL-GFP within the SLB, we introduced TEV protease into the device to assess protein orientation. TEV should cleave GFP

https://doi.org/10.1021/acssynbio.2c00531
ACS Synth. Biol. 2023, 12, 502−510

from the transmembrane protein only if it has adopted the correct orientation within the membrane, with the GFP accessible and facing the bulk phase. After treatment with the TEV protease, we observed a nearly 90% reduction in the number of individual fluorescent spots, indicating that MscL-GFP is being co-translationally synthesized into the SLB predominantly in one orientation (Figure 2A).

After determining the orientation of MscL-GFP, we performed a second set of experiments to assess protein mobility in these fluid SLBs using single-particle tracking analysis. A representative image and the trajectories of mobile particles in the frame is shown in Figure 2B, and representative MSD plots are shown in Figure S5 (Supporting Information). We measured the trajectories of individual MscL-GFP molecules and calculated the mean square displacement (MSD) to determine local diffusion coefficients. We used the initial slope from the first three time points to determine the diffusivity in the local region of MscL-GFP. We plotted these diffusion coefficients as a histogram and fit the data with a gamma distribution to determine the mean diffusion coefficient for the population (Figure 2B). We found that the mobile proteins have an average diffusion coefficient of 0.18 ± 0.07 $\mu m^2/s$ with an overall mobile fraction of 0.37 ± 0.03 (which means roughly 40% of proteins have mobility). This diffusion coefficient and mobile fraction suggest that the polymer layer is providing a "cushioning" effect here that maintains mobility for proteins that are synthesized into the bilayer plane. The fluorescence of the GFP folding reporter, accessibility of the C-terminal TEV cleavage site as a readout of protein orientation, and protein mobility together indicate that the channel is fully integrated and adopts a native-like conformation in the SLB on the PEDOT:PSS support. These data provide further experimental validation that the supported lipid membrane is contiguous on the surface given the length scale of the protein diffusion.

Electrochemical Impedance Spectroscopy Confirms the Function of MscL Channels. After confirming the insertion, orientation, and mobility of our target protein using fluorescence, we used electrochemical impedance spectroscopy (EIS) to functionally characterize the performance of our biosensor. To determine whether MscL ion channels synthesized into supported bilayers using cell-free methods were functional, we utilized our electrode platform to sense the ion flux activity across the bilayer using label-free electrical methods. To assess the specificity of protein responses, we used a previously characterized mutant version of the MscL protein (G22C-MscL). This point mutation (Gly-22 to Cys-22) puts a sulfhydryl group on each subunit of the channel, making G22C-MscL responsive to methanethiosulfonate (MTS) reagents.[23,37] Addition of MTS therefore triggers the opening of the G22C channel. In contrast, the wild-type (WT) version of MscL is not activated by this chemical.

We monitored the EIS response at critical stages of electrode functionalization using Nyquist plots (Figure 3). The corresponding Bode and phase representations of the data are shown in Figure S6 (Supporting Information). First, we obtained the impedance spectra of PAH-coated PEDOT:PSS ITO electrodes alone as a baseline for the device. Next, we incubated POPC−POPG liposomes on the electrode surfaces and monitored the formation of a POPC−POPG bilayer via an increase in the impedance values (red data sets) from the bare electrode. This increase in impedance corresponds to the formation of a lipid bilayer that then impedes the flux of ions to the electrode.

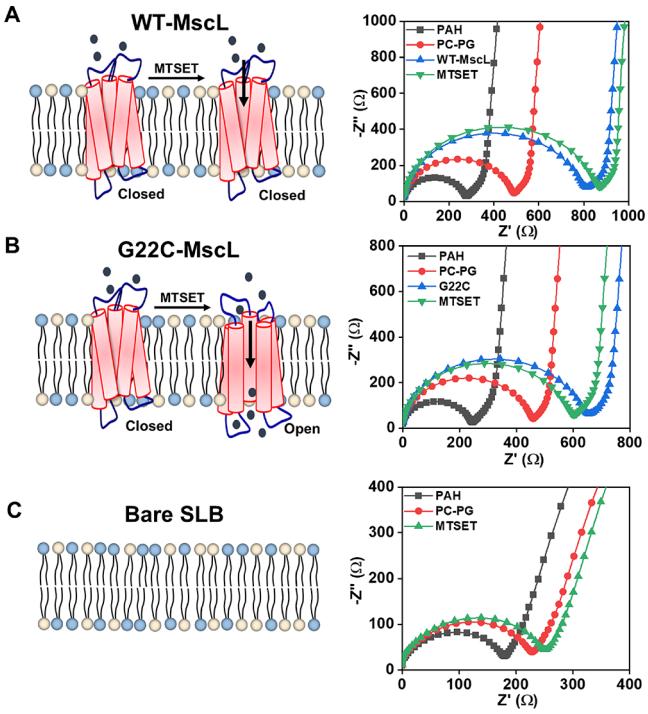

Figure 3. Impedance monitoring to show the channel activity of WT and mutant (G22C) MscL-containing SLBs on a PAH/PEDOT:PSS-coated ITO electrode. Schematics and Nyquist plots of POPC−POPG bilayer formation (red), protein synthesis (blue), and interaction with MTSET (green) (10 μM) are presented for (A) WT-MscL (channel remains closed), (B) G22C-MscL (channels open), and (C) bare SLB (no channel).

We then integrated MscL into the membrane. On separate electrodes, we synthesized WT-MscL, and the chemically activatable mutant (G22C-MscL) into SLBs and EIS spectra were taken prior to MTSET addition. In both cases, the impedance spectra shifted to higher resistance values, consistent with increased packing within the bilayer upon insertion of protein (blue data sets). Although the reactions were run for the same amount of time and under the same conditions (plasmid concentration, synthesis reagents, etc.), there was occasional variation in the overall increase in impedance. However, these small differences are not statistically significant and do not affect the ability to detect protein expression nor to measure protein activity and response to MTSET. The insertion of WT-MscL and G22C-MscL increased the R_m by 80 ± 10 and 90 ± 40%, respectively (Supporting Information, Table S1). We confirmed this by comparing the fluorescence signals from both G22C-MscL and WT-MscL folding and observed no difference in the incorporation efficiency (Supporting Information, Figure S7−S8).

After cell-free expression of the WT- and G22C-MscL into our SLBs, we exposed them to the chemical activator MTSET to study their function. We monitored the channel activity during addition of MTSET as changes in membrane resistance. Regardless of the starting impedance, the addition of MTSET is known to trigger the opening of the mutant G22C-MscL channel and in turn should lower membrane impedance, while the WT-MscL channel should remain unaffected by addition of MTSET. Accordingly, after addition of MTSET to the G22C-

https://doi.org/10.1021/acssynbio.2c00531
ACS Synth. Biol. 2023, 12, 502−510

MscL- and WT-MscL-integrated membranes, we observed distinct electrical responses that are consistent with the expected channel activities in each case. The spectra shown in Figure 3A,B are representative of the expected results for these cases; when the channels are open, there is increased ion flow. For the G22C-MscL integrated membranes, we observe a shift in the impedance to lower values, indicating that the resistance has indeed dropped, presumably due to the opening of the ion channels triggered by MTSET. For WT-MscL, we do not observe this drop in the presence of MTSET and instead see a slight increase in impedance. To interpret the results, we next monitored the effect of MTSET on a bare SLB without protein. We observed an increase in impedance (Figure 3C) after addition to the membrane. One plausible explanation for this observed increase is that MTSET, which is positively charged, is interacting with the anionic SLB. Other reports have used EIS to detect charged molecules interacting with a membrane or surface, showing that this explanation is a possibility in our system as well.[38,39] Based on the previous inherent impedance change from the bare SLB, we were able to correct the impedance changes to reflect this intrinsic response. Most importantly, the lower impedance values observed with G22C-MscL indicate that these channels are functional, chemically specific, and responsive to MTSET.

Within the same working electrode, there is a clear distinction between the impedance response of G22C-MscL and WT-MscL after MTSET addition. To compare the observed responses across different devices, we fit the data to an equivalent circuit and calculated the membrane properties, (i.e., resistance and capacitance) of the supported membranes in each case and the changes in response to MTSET. The equivalent model circuit is depicted in Figure 4A, where the

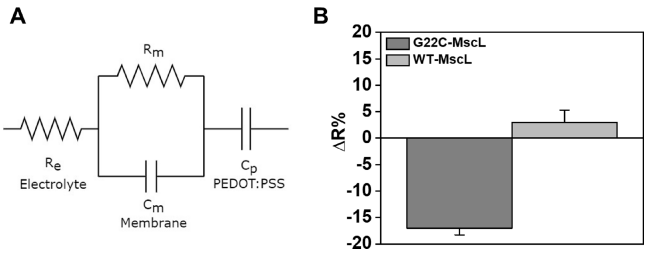

Figure 4. Impedance measurements were analyzed to calculate membrane electrical properties. (A) Equivalent circuit diagram representing each component in the system. (B) Relative change in resistance after the addition of MTSET in either WT or G22C incorporated SLBs, accounting for the effect of MTSET on a bare SLB. Error bars represent standard error of the mean, $n = 3$.

membrane is represented as an RC circuit in series with a resistor for the electrolyte and a capacitor element for the conducting polymer layer.[16] This circuit is representative of the physical properties of the sensing system.[27] The resistance and capacitance for membrane components for each sample in all three cases are given in Table S1, Supporting Information.

When WT-MscL was exposed to MTSET, we observed a 3% increase on average in resistance across three separate experiments when compared to baseline MTSET effects (Figure 4B). Because there are no interaction sites for MTSET, the cause of this increase in impedance is likely non-specific interactions. For G22C-MscL, we observe an 18% decrease in the membrane resistance relative to the baseline effect of MTSET. The individual values are provided in Table S2, Supporting Information. This decrease in the membrane resistance is presumably due to the activation and opening of the channel by MTSET as compared with the wild-type case. The electrolyte resistance and PEDOT:PSS capacitance are unaffected during this process (Table S3, Supporting Information). To provide further validation that we are observing specific protein activation, we conducted a mathematical analysis on our observed resistance changes. This matches with our observed protein counts obtained using fluorescence imaging (Supporting Information). Taken together, these results validate CFPS methods as a viable approach to producing functional, biologically complex proteins in vitro in sensing devices capable of optical and electrical readouts.

CONCLUSIONS

We describe here the combination of a biomembrane-based electronic biosensor with cell-free protein synthesis as a platform to rapidly integrate functional transmembrane proteins and assess their activity. We first demonstrate that we can easily fabricate SLBs on a conducting polymer support. Then, using a well-studied bacterial TMP (MscL), we show that we can incorporate a mobile membrane protein into SLBs in these devices using a one-step cell-free protein synthesis reaction, bypassing purification and reconstitution. Crucially, we demonstrate with our device, in conjunction with a chemically responsive MscL mutant (G22C-MscL), that we can monitor ion channel activity upon treatment with a chemical activator. These observations indicate that cell-free synthesis can directly integrate membrane proteins as sensing elements and create a suitable biosensor interface.

By using commercial ITO electrodes with the widely used, biocompatible, and transparent PEDOT:PSS coating, this biosensor platform is easily assembled and proteins are readily integrated using cell free protein synthesis. Protein activity, orientation, and mobility are key features in native biological function that we retain in our biosensor platform and are easily assayed by fluorescence microscopy. As such, this biosensor preserves the ability to assess biophysical properties of the protein and membrane, which leaves open the possibility of using fluorescence to study some aspects of the target protein and a label-free electrical readout for others. Therefore, an exciting possibility for the future is the simultaneous readout of optical and electrical signals that can potentially be leveraged for the single molecule resolution of protein activity.

Using this cell-free protein expression system, we can rapidly integrate specific and active transmembrane proteins into the biosensor interface and measure membrane protein activity. This approach can be done without the need for cell culture, protein purification, or other intensive procedures that are typically required to construct transmembrane protein-based biosensors. Such accessible fabrication will further expand the adoption and innovation of biosensing platforms. Recently, other modalities of biosensing capabilities have shown potential as well, for example with membrane droplets[40] or freestanding membranes.[41] With our configuration, however, we can provide customized circuit design for any electrical configuration and great ease of use by using vesicle fusion techniques. We also envision that our technique can be applied to a wide range of transmembrane proteins, potentially even in a single device. This would enable the creation of a robust sensor able to detect a broad range of different molecules.

https://doi.org/10.1021/acssynbio.2c00531
ACS Synth. Biol. 2023, 12, 502−510

By dramatically simplifying TMP synthesis and biosensor fabrication, this platform is poised to provide a convenient tool to study protein function in this age of biotechnology. For example, synthetic additives can be added to modify the proteins in a way not possible using cell culture methods, or reactions can be scaled to vary protein expression levels. Furthermore, by employing a cell-free environment, large libraries of protein variants can be easily synthesized and introduced using microfluidic environments, both of which will be critical in building advanced biosensors. Overlaying these advances with the massive parallelization possible with microfluidics will enable the scaling-up needed to rapidly screen for TMP activity beyond what is currently feasible. This enables a broad spectrum of applications that are at the forefront of biotechnology research and that benefit from transmembrane protein studies, including the evaluation of protein structure−function relationships, the development of drug discovery pipelines that screen the effect of therapeutics on membrane proteins, and the development of multiplexed biosensors.

■ ASSOCIATED CONTENT

Supporting Information

The Supporting Information is available free of charge at https://pubs.acs.org/doi/10.1021/acssynbio.2c00531.

Characterization of POPC-POPG liposomes: intensity-size distribution, average diameter, and ζ potential; fluidity of POPC-POPG SLBs formed on glass, PEDOT:PSS, or PAH surfaces using TR-DHPE as the reporting fluorophore; quantification of membrane fluidity of POPC−POPG SLBs on the PAH/glass surface; comparison of the diffusion coefficient and mobile fraction of TR-DHPE in PAH/glass and PAH/PEDOT:PSS surfaces; mean square displacement (MSD) measurements of diffusive protein motion; EIS response following MTSET addition to MscL-integrated POPC−POPG SLBs on PAH/PEDOT:PSS coated ITO electrodes; comparison of WT-MscL and G22C-MscL incorporation; modeling of EIS data to extract membrane components; analysis of protein resistance and incorporation (PDF)

■ AUTHOR INFORMATION

Corresponding Author

Susan Daniel − *R.F. School of Chemical and Biomolecular Engineering, Cornell University, Ithaca, New York 14853, United States;* orcid.org/0000-0001-7773-0835; Email: sd386@cornell.edu

Authors

Zachary A. Manzer − *R.F. School of Chemical and Biomolecular Engineering, Cornell University, Ithaca, New York 14853, United States;* orcid.org/0000-0002-8225-8990

Surajit Ghosh − *R.F. School of Chemical and Biomolecular Engineering, Cornell University, Ithaca, New York 14853, United States;* orcid.org/0000-0003-1045-5191

Arpita Roy − *R.F. School of Chemical and Biomolecular Engineering, Cornell University, Ithaca, New York 14853, United States*

Miranda L. Jacobs − *Department of Biomedical Engineering and Interdisciplinary Biological Sciences Program, Northwestern University, Evanston, Illinois 60208, United States*

Juliana Carten − *R.F. School of Chemical and Biomolecular Engineering, Cornell University, Ithaca, New York 14853, United States*

Neha P. Kamat − *Department of Biomedical Engineering, Center for Synthetic Biology, Northwestern University, Evanston, Illinois 60208, United States;* orcid.org/0000-0001-9362-6106

Complete contact information is available at: https://pubs.acs.org/10.1021/acssynbio.2c00531

Author Contributions

‖Z.A.M. and S.G. contributed equally to this work.

Author Contributions

Z.A.M. and S.G. conceived the original idea. Z.A.M., S.G., and A.R. conducted experiments and analyzed the data. Z.A.M., S.G., A.R., and S.D. drafted the manuscript. Z.A.M., S.G., A.R., M.L.J., J.C., N.P.K., and S.D. edited the manuscript. All authors have given approval to the final version of the manuscript.

Notes

The authors declare no competing financial interest.

■ ACKNOWLEDGMENTS

This work was supported by the NSF grant MCB-1935356 (S.D. and N.P.K.) and the Air Force Office of Scientific Research (AFOSR) YIP FA9550-19-1-0039 P00001 (N.P.K.). M.L.J. is supported by an American Heart Association Predoctoral Fellowship (grant no. 20PRE35180215). The project described was supported by T32GM138826 from the National Institute of General Medical Sciences (ZAM). The content is solely the responsibility of the authors and does not necessarily represent the official views of the National Institute of General Medical Sciences or the National Institutes of Health. Z.A.M. was supported by a School of Chemical and Biomolecular Engineering Fleming Fellowship. S.D. acknowledges funding for this project sponsored by the Defense Advanced Research Projects Agency (DARPA) Army Research Office and accomplished under Cooperative Agreement Number W911NF-18-2-0152. The views and conclusions contained in this document are those of the authors and should not be interpreted as representing the official policies, either expressed or implied, of DARPA or the Army Research Office or the U.S. Government. The U.S. Government is authorized to reproduce and distribute reprints for Government purposes notwithstanding any copyright notation herein.

■ REFERENCES

(1) Li, P.; Lee, G. H.; Kim, S. Y.; Kwon, S. Y.; Kim, H. R.; Park, S. From Diagnosis to Treatment: Recent Advances in Patient-Friendly Biosensors and Implantable Devices. *ACS Nano* **2021**, *15*, 1960−2004.

(2) Santoro, F.; Lubrano, C.; Matrone, G. M.; Iaconis, G. New Frontiers for Selective Biosensing with Biomembrane-Based Organic Transistors. *ACS Nano* **2020**, *14*, 12271−12280.

(3) Gong, H.; Chen, F.; Huang, Z.; Gu, Y.; Zhang, Q.; Chen, Y.; Zhang, Y.; Zhuang, J.; Cho, Y. K.; Fang, R. H.; Gao, W.; Xu, S.; Zhang, L. Biomembrane-Modified Field Effect Transistors for Sensitive and Quantitative Detection of Biological Toxins and Pathogens. *ACS Nano* **2019**, *13*, 3714−3722.

(4) Inal, S.; Rivnay, J.; Suiu, A. O.; Malliaras, G. G.; McCulloch, I. Conjugated Polymers in Bioelectronics. *Acc. Chem. Res.* **2018**, *51*, 1368−1376.

(5) Ang, P. K.; Jaiswal, M.; Lim, C. H. Y. X.; Wang, Y.; Sankaran, J.; Li, A.; Lim, C. T.; Wohland, T.; Barbaros, Ö.; Loh, K. P. A Bioelectronic Platform Using a Graphene-Lipid Bilayer Interface. *ACS Nano* **2010**, *4*, 7387−7394.
(6) Koklu, A.; Wustoni, S.; Musteata, V. E.; Ohayon, D.; Moser, M.; McCulloch, I.; Nunes, S. P.; Inal, S. Microfluidic Integrated Organic Electrochemical Transistor with a Nanoporous Membrane for Amyloid-β Detection. *ACS Nano* **2021**, 8130.
(7) Jayaram, A. K.; Pappa, A. M.; Ghosh, S.; Manzer, Z. A.; Traberg, W. C.; Knowles, T. P. J.; Daniel, S.; Owens, R. M. Biomembranes in Bioelectronic Sensing. *Trends Biotechnol.* **2022**, 1−123.
(8) Gözen, I.; Jesorka, A. Instrumental Methods to Characterize Molecular Phospholipid Films on Solid Supports. *Anal. Chem.* **2012**, *84*, 822−838.
(9) Cho, N.-J.; Frank, C. W.; Kasemo, B.; Höök, F. Quartz Crystal Microbalance with Dissipation Monitoring of Supported Lipid Bilayers on Various Substrates. *Nat. Protoc.* **2010**, *5*, 1096−1106.
(10) Liu, H. Y.; Pappa, A. M.; Pavia, A.; Pitsalidis, C.; Thiburce, Q.; Salleo, A.; Owens, R. M.; Daniel, S. Self-Assembly of Mammalian-Cell Membranes on Bioelectronic Devices with Functional Transmembrane Proteins. *Langmuir* **2020**, *36*, 7325−7331.
(11) Mashaghi, A.; Mashaghi, S.; Reviakine, I.; Heeren, R. M. A.; Sandoghdar, V.; Bonn, M. Label-Free Characterization of Biomembranes: From Structure to Dynamics. *Chem. Soc. Rev.* **2014**, *43*, 887−900.
(12) Liu, H. Y.; Pappa, A. M.; Hidalgo, T. C.; Inal, S.; Owens, R. M.; Daniel, S. Biomembrane-Based Organic Electronic Devices for Ligand−Receptor Binding Studies. *Anal. Bioanal. Chem.* **2020**, 6265.
(13) Bint E Naser, S. F.; Su, H.; Liu, H. Y.; Manzer, Z. A.; Chao, Z.; Roy, A.; Pappa, A.-M.; Salleo, A.; Owens, R. M.; Daniel, S. Detection of Ganglioside-Specific Toxin Binding with Biomembrane-Based Bioelectronic Sensors. *ACS Appl. Bio Mater.* **2021**, *4*, 7942−7950.
(14) Tang, T.; Savva, A.; Traberg, W. C.; Xu, C.; Thiburce, Q.; Liu, H.-Y.; Pappa, A.-M.; Martinelli, E.; Withers, A.; Cornelius, M.; Salleo, A.; Owens, R. M.; Daniel, S. Functional Infectious Nanoparticle Detector: Finding Viruses by Detecting Their Host Entry Functions Using Organic Bioelectronic Devices. *ACS Nano* **2021**, 18142.
(15) Yoon, B. K.; Jeon, W. Y.; Sut, T. N.; Cho, N. J.; Jackman, J. A. Stopping Membrane-Enveloped Viruses with Nanotechnology Strategies: Toward Antiviral Drug Development and Pandemic Preparedness. *ACS Nano* **2021**, *15*, 125−148.
(16) Pappa, A. M.; Liu, H. Y.; Traberg-Christensen, W.; Thiburce, Q.; Savva, A.; Pavia, A.; Salleo, A.; Daniel, S.; Owens, R. M. Optical and Electronic Ion Channel Monitoring from Native Human Membranes. *ACS Nano* **2020**, *14*, 12538−12545.
(17) Kruyer, N. S.; Sugianto, W.; Tickman, B. I.; Alba Burbano, D.; Noireaux, V.; Carothers, J. M.; Peralta-Yahya, P. Membrane Augmented Cell-Free Systems: A New Frontier in Biotechnology. *ACS Synth. Biol.* **2021**, *10*, 670−681.
(18) Soranzo, T.; Martin, D. K.; Lenormand, J. L.; Watkins, E. B. Coupling Neutron Reflectivity with Cell-Free Protein Synthesis to Probe Membrane Protein Structure in Supported Bilayers. *Sci. Rep.* **2017**, *7*, 1−10.
(19) Chadli, M.; Rebaud, S.; Maniti, O.; Tillier, B.; Cortès, S.; Girard-Egrot, A. New Tethered Phospholipid Bilayers Integrating Functional G-Protein-Coupled Receptor Membrane Proteins. *Langmuir* **2017**, *33*, 10385−10401.
(20) Manzer, Z. A.; Ghosh, S.; Jacobs, M. L.; Krishnan, S.; Zipfel, W. R.; Piñeros, M.; Kamat, N. P.; Daniel, S. Cell-Free Synthesis of a Transmembrane Mechanosensitive Channel Protein into a Hybrid-Supported Lipid Bilayer. *ACS Appl. Bio Mater.* **2021**, acsabm.0c01482.
(21) Booth, I. R.; Blount, P. The MscS and MscL Families of Mechanosensitive Channels Act as Microbial Emergency Release Valves. *J. Bacteriol.* **2012**, *194*, 4802−4809.
(22) Jacobs, M. L.; Boyd, M. A.; Kamat, N. P. Diblock Copolymers Enhance Folding of a Mechanosensitive Membrane Protein during Cell-Free Expression. *Proc. Natl. Acad. Sci.* **2019**, *116*, 201814775.
(23) Yoshimura, K.; Batiza, A.; Kung, C. Chemically Charging the Pore Constriction Opens the Mechanosensitive Channel MscL. *Biophys. J.* **2001**, *80*, 2198−2206.
(24) Soumpasis, D. M. Theoretical Analysis of Fluorescence Photobleaching Recovery Experiments. *Biophys. J.* **1983**, *41*, 95−97.
(25) Schneider, C. A.; Rasband, W. S.; Eliceiri, K. W. NIH Image to ImageJ: 25 Years of Image Analysis. *Nat. Methods* **2012**, *9*, 671−675.
(26) Berggren, M.; Malliaras, G. G. How Conducting Polymer Electrodes Operate. *Science* **2019**, *364*, 233−234.
(27) Lu, Z.; van Niekerk, D.; Savva, A.; Kallitsis, K.; Thiburce, Q.; Salleo, A.; Pappa, A. M.; Owens, R. M. Understanding Electrochemical Properties of Supported Lipid Bilayers Interfaced with Organic Electronic Devices. *J. Mater. Chem. C* **2022**, *10*, 8050−8060.
(28) Leleux, P.; Johnson, C.; Strakosas, X.; Rivnay, J.; Hervé, T.; Owens, R. M.; Malliaras, G. G. Ionic Liquid Gel-Assisted Electrodes for Long-Term Cutaneous Recordings. *Adv. Healthcare Mater.* **2014**, *3*, 1377−1380.
(29) Dijk, G.; Rutz, A. L.; Malliaras, G. G. Stability of PEDOT:PSS-Coated Gold Electrodes in Cell Culture Conditions. *Adv. Mater. Technol.* **2020**, *5*, 1900662.
(30) Diamanti, E.; Gregurec, D.; Rodríguez-Presa, M. J.; Gervasi, C. A.; Azzaroni, O.; Moya, S. E. High Resistivity Lipid Bilayers Assembled on Polyelectrolyte Multilayer Cushions: An Impedance Study. *Langmuir* **2016**, *32*, 6263−6271.
(31) Fischlechner, M.; Zaulig, M.; Meyer, S.; Estrela-Lopis, I.; Cuéllar, L.; Irigoyen, J.; Pescador, P.; Brumen, M.; Messner, P.; Moya, S.; Donath, E. Lipid Layers on Polyelectrolyte Multilayer Supports. *Soft Matter* **2008**, *4*, 2245−2258.
(32) Pappa, A. M.; Inal, S.; Roy, K.; Zhang, Y.; Pitsalidis, C.; Hama, A.; Pas, J.; Malliaras, G. G.; Owens, R. M. Polyelectrolyte Layer-by-Layer Assembly on Organic Electrochemical Transistors. *ACS Appl. Mater. Interfaces* **2017**, *9*, 10427−10434.
(33) Zhang, L.; Vidu, R.; Waring, A. J.; Lehrer, R. I.; Longo, M. L.; Stroeve, P. Electrochemical and Surface Properties of Solid-Supported, Mobile Phospholipid Bilayers on a Polyion/Alkylthiol Layer Pair Used for Detection of Antimicrobial Peptide Insertion. *Langmuir* **2002**, *18*, 1318−1331.
(34) Decher, G.; Hong, J. D.; Schmitt, J. Buildup of Ultrathin Multilayer Films by a Self-Assembly Process: III. Consecutively Alternating Adsorption of Anionic and Cationic Polyelectrolytes on Charged Surfaces. *Thin Solid Films* **1992**, *210-211*, 831−835.
(35) Waldo, G. S.; Standish, B. M.; Berendzen, J.; Terwilliger, T. C. Rapid Protein-Folding Assay Using Green Fluorescent Protein. *Nat. Biotechnol.* **1999**, *17*, 691−695.
(36) Jacobs, M. L.; Boyd, M. A.; Kamat, N. P. Diblock Copolymers Enhance Folding of a Mechanosensitive Membrane Protein during Cell-Free Expression. *Proc. Natl. Acad. Sci. U. S. A.* **2019**, *116*, 4031−4036.
(37) Batiza, A. F.; Kuo, M. M. C.; Yoshimura, K.; Kung, C. Gating the Bacterial Mechanosensitive Channel MscL in Vivo. *Proc. Natl. Acad. Sci. U. S. A.* **2002**, *99*, 5643−5648.
(38) Fritz, J.; Cooper, E. B.; Gaudet, S.; Sorger, P. K.; Manalis, S. R. Electronic Detection of DNA by Its Intrinsic Molecular Charge. *Proc. Natl. Acad. Sci.* **2002**, *99*, 14142−14146.
(39) Magar, H. S.; Hassan, R. Y. A.; Mulchandani, A. Electrochemical Impedance Spectroscopy (EIS): Principles, Construction, and Biosensing Applications. *Sensors* **2021**, *21*, 6578.
(40) Strutt, R.; Hindley, J. W.; Gregg, J.; Booth, P. J.; Harling, J. D.; Law, R. V.; Friddin, M. S.; Ces, O. Activating Mechanosensitive Channels Embedded in Droplet Interface Bilayers Using Membrane Asymmetry. *Chem. Sci.* **2021**, 2138−2145.
(41) Ensslen, T.; Behrends, J. C. A Chip-Based Array for High-Resolution Fluorescence Characterization of Free-Standing Horizontal Lipid Membranes under Voltage Clamp. *Lab Chip* **2022**, *22*, 2902−2910.

https://doi.org/10.1021/acssynbio.2c00531
ACS Synth. Biol. 2023, 12, 502−510